Chapter 2
Redoximorphic Features in Albeluvisols from South-Western Ukraine

Volodymyr Nikorych, Wojciech Szymański and Michał Skiba

Abstract Polarizing microscopy and scanning electron microscopy were used to determine the distribution, size, shape, and chemical composition of Fe–Mn nodules in *Albeluvisols (Retisols)* from south-western Ukraine and the relationship of these pedological features with redox processes. Intrusive, impregnative, and depletion features were observed. The highest content of hard nodules is present in the upper part of the solum, indicating that cyclic redox processes occur most often above the illuvial horizon. The nodules are enriched in Fe and Mn (4–14 and 7–40 times, respectively). The chemical composition of the surface of the nodule in contact with microorganisms indicates their crucial role in the accumulation of Fe and Mn and nodule formation.

Keywords Fe–Mn nodules · Fe–Mn concretions · Redox · Albeluvisols · Micromorphology · Scanning electron microscopy

Introduction

Concentrations of iron and manganese compounds in soils may occur as pedofeatures such as nodules and coatings of various shapes and sizes. Fe–Mn nodules and concretions are solid and easily observed and are important in soil diagnostics

V. Nikorych (✉)
Department of Soil Science, Yuri Fedkovich Chernivtsi National University,
L. Ukrainki 25, Chernivtsi 58000, Ukraine
e-mail: v.nikorych@chnu.edu.ua

W. Szymański
Department of Pedology and Soil Geography, Institute of Geography and Spatial Management, Jagiellonian University, Gronostajowa 7, 30-387 Kraków, Poland

M. Skiba
Department of Mineralogy, Petrology and Geochemistry, Institute of Geological Sciences, Jagiellonian University, Oleandry 2a, 30-063 Kraków, Poland

D. Dent and Y. Dmytruk (eds.), *Soil Science Working for a Living*,
DOI 10.1007/978-3-319-45417-7_2

—especially in identifying redox conditions (Zhang and Karathanasis 1997; Vepraskas 2001; Gasparatos et al. 2005). They accumulate elements of variable valency and control the distribution and mobility of cations in the soil (Suarez and Langmuir 1976). In a sense, they are the memory of the soil and throw light on its genesis (Zaidelman and Nikiforova 2010).

Many and various Fe–Mn pedofeatures are described in the literature: glaebules, septaria, ferricretes (Brewer 1964), stains, ortsands, ortsteins, concretions, and nodules (Zaidelman and Nikiforova 2001, 2010; Lindbo et al. 2010; Szendrei et al. 2012; Szymański and Skiba 2013; Nikorych et al. 2014). The different terms refer to the variety of form, composition, genesis and, sometimes, national traditions in the absence of a common classification of these features. For instance, Zaidelman and Nikiforova (2001) distinguish classes (concretional and non-concretional), types (based on chemical composition), families (based on form), and species (based on morphology), but there are several other informative and logical systems.

Most Fe–Mn redoximorphic pedofeatures are discrete, hard bodies characterized by a specific colour and often called ortstein, concretions, and nodules. Various terms are used synonymously, but recent studies with polarizing and scanning electron microscopes reveal two distinct types: (1) showing a relatively uniform distribution of Fe (oxyhydr)oxides and Mn oxides and (2) showing internal structure with concentric bands or layers of different content of Fe (oxyhydr)oxides and Mn oxides. Hickey et al. (2008) distinguish nodules and concretions, arguing that the different forms indicate different genesis; we might also consider differences in parent material, moisture regime, climatic conditions, as well as the quantity and kind of soil organisms.

Fe (oxyhydr)oxides and Mn oxides adsorb various elements including trace metals (Ti, Cu, Co, Cr, Ni, Pb, Zn), phosphorus and carbon, and play a role in many soil chemical reactions (Schwertmann and Fanning 1976; Latrille et al. 2001; Palumbo et al. 2001; Tan et al. 2006; Huang et al. 2008; Cornu et al. 2009; Sipos et al. 2011; Szymański and Skiba 2013).

Here, we determine the distribution, size, shape, and chemical composition of Fe–Mn pedofeatures and consider their relationship with redox processes in Albeluvisols from the south-western part of Ukraine. To understand their formation and evolution, we calculate the enrichment factor (EF) as the ratio of the concentration of the chemical elements in the studied feature to their concentration in the soil matrix. Many studies indicate that EF depends on the large specific surface and pH-dependent surface charge of Fe (oxyhydr)oxides and Mn oxides (Schwertmann and Fanning 1976; Dawson et al. 1985; Tan et al. 2006; Zaidelman and Nikiforova 2010; Szymański and Skiba 2013).

Materials and Methods

Study Area

The study was carried out in the Precarpathians of south-western Ukraine (Fig. 2.1)—an undulating landscape with broad hills rising to 600 m above sea level. The bedrock is flysch, covered by up to 25 m of non-calcareous loess. Mean annual temperature is 6–8 °C; mean annual precipitation is 650–800 mm. Most of the area is forested with oak (*Quercus* spp.), beech (*Fagus sylvatica* L.), fir (*Abies alba* Mill.), hornbeam (*Carpinus betulus* L.), lime (*Tilia cordata* Mill.), larch (*Larix decidua* Mill.), and willow (*Salix* spp.), but quite large areas are cultivated. The soils are mostly Luvisols and Albeluvisols (IUSS Working Group WRB 2006) or Retisols (IUSS Working Group WRB 2014); the lack of carbonates in the parent material and the humid climate encourage wash-down of clay from the upper to the middle part of the soil profile (Quénard et al. 2011).

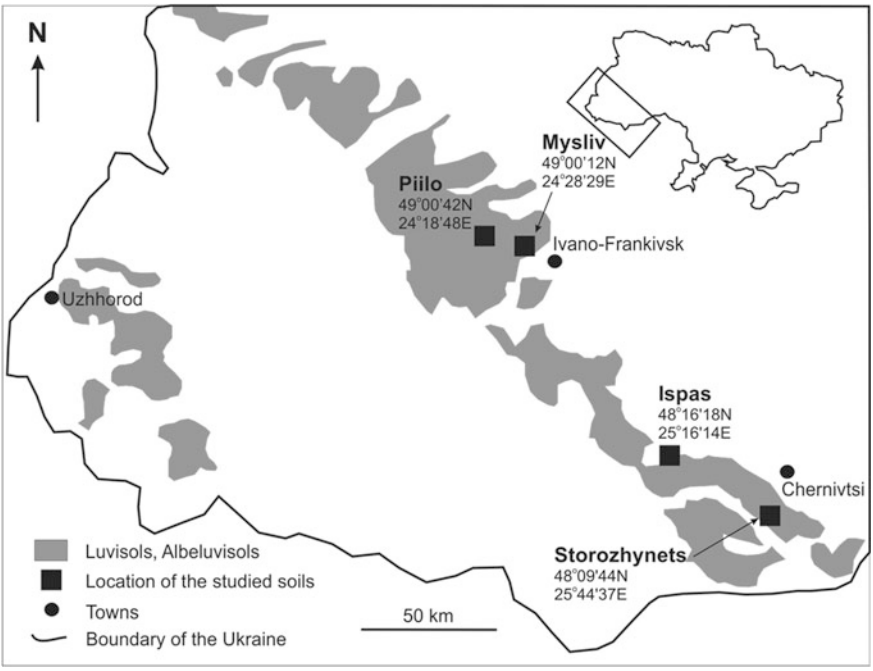

Fig. 2.1 Occurrence of Luvisols and Albeluvisols in SW Ukraine and location of soil profiles

Field and Laboratory Methods

From 20 described soil profiles, four representatives were selected for detailed analysis (Fig. 2.1; Tables 2.1 and 2.2), all classified as Stagnic Fragic Albeluvisols (Siltic). The Piilo profile is under deciduous forest, the Ispas and Mysliv profiles are under mixed forest, and the Storozhynets profile is under coniferous forest. Detailed profile descriptions are given by Nikorych et al. (2014).

From each soil horizon, undisturbed samples were collected for micromorphological study and bulk samples for physical and chemical analysis. The latter were air-dried and sieved through a 1-mm sieve; laboratory analyses were conducted on the fine earth fraction (<1 mm).

Fe–Mn nodules were separated by boiling 40 g of fine earth for 30 min in 600 ml distilled water containing 1.5 g Na_2CO_3 as a dispersant. After boiling, the samples were wet-sieved through 0.5, 0.25, and 0.1-mm sieves and oven-dried at 105 °C for 24 h. The separated fractions were weighed. Coarse Fe–Mn nodules (1–0.5 mm) were hand-picked under a magnifying glass. These were weighed again. The medium (0.5–0.25 mm) and fine (0.25–0.1 mm) fractions were treated with 10% HCl for 24 h to remove Fe–Mn nodules, washed three times with distilled water to remove dissolved Fe (oxyhydr)oxides and Mn oxides, then oven-dried at 105 °C for 24 h, and weighed. Soil organic carbon content was determined by rapid dichromate oxidation (Nelson and Sommers 1996); pH was measured potentiometrically in distilled water using a 1:2.5 soil/water ratio; the concentration of Fe and Al in ammonium oxalate extracts prepared according to Tamm's procedure was determined using a UV–Vis spectrometer. Particle size distribution was determined by sieving and hydrometer methods. Bulk density and total porosity were measured on undisturbed cores.

A Nikon Eclipse E600POL polarizing microscope was used for micromorphological studies; thin sections were described following Stoops (2003). Image analyses of micrographs employed MultiscanBase v.18.03 software using the colour of the studied pedofeatures. Separated coarse Fe–Mn nodules (and aggregates for comparison) were observed and analysed under a Hitachi S-4700 field emission scanning electron microscope (FESEM) equipped with a Vantage Noran energy dispersive X-ray spectroscopy (EDS) system. Details of sample preparation for FESEM–EDS studies can be found in Szymański and Skiba (2013). The relative chemical composition of the nodules and aggregates (point and area analyses in not less than 10 repeats) was determined with the application of an acceleration voltage of 20 kV, an emission current of 10 μA, and a 100 s count time.

Table 2.1 Profile descriptions

Horizon	Depth (cm)	Munsell colour (moist)	Structure	Consistence	Roots	Clay coatings
Storozhynets						
O	0–5	n.a.	n.a.	n.a.	n.a.	n.a.
AEg	5–22	10YR 5/3	Subangular blocky	Soft	Few	Absent
Eg	22–33	10YR 5/4	Subangular blocky	Slightly hard	Few	Few
Btx	33–60	10YR 5/6; 10YR 6/2	Prismatic	Hard	None	Many
2Btg	60–100	10YR 5/6; 10YR 6/2	Prismatic	Hard	None	Many
2BC	>100	10YR 5/6; 10YR 8/1	Massive	Very hard	None	Common
Ispas						
A	0–6	n.a.	n.a.	n.a.	n.a.	n.a.
AEg	6–15	10YR 5/3	Subangular blocky	Slightly hard	Many	Absent
Eg	15–32	10YR 5/4	Subangular blocky	Slightly hard	Few	Few
Btx1	32–52	10YR 5/6; 10YR 6/2	Prismatic	Very hard	Few	Common
Btx2	52–110	10YR 5/6; 10YR 6/2	Prismatic	Very hard	None	Many
Btg	110–140	10YR 5/4	Prismatic	Very hard	None	Common
Mysliv						
O	0–2	n.a.	n.a.	n.a.	n.a.	n.a.
A	2–14	10YR 4/2	Subangular blocky	Soft	Many	Few
Eg	14–30	10YR 5/4	Massive	Slightly hard	Common	Absent
Btx1	30–49	10YR 5/4; 10YR 6/2	Blocky	Very hard	Few	Common
Btx2	49–57	10YR 5/3; 10YR 6/2	Prismatic	Very hard	Few	Many
Btx3	57–120	10YR 5/3; 10YR 6/2	Prismatic	Very hard	None	Common
Piilo						
O	0–6	n.a.	n.a.	n.a.	n.a.	n.a.
A	6–16	10YR 4/2	Subangular blocky	Slightly hard	Many	Absent
AE	16–31	10YR 5/2	Blocky	Slightly hard	Common	Absent

(continued)

Table 2.1 (continued)

Horizon	Depth (cm)	Munsell colour (moist)	Structure	Consistence	Roots	Clay coatings
Eg	31–43	10YR 5/2	Blocky	Slightly hard	Few	Few
Btx1	43–72	10YR 5/3; 10YR 6/3	Prismatic	Very hard	Few	Common
Btx2	72–110	10YR 4/3; 10YR 6/3	Prismatic	Very hard	None	Many
BC	110–123	10YR 4/3; 10YR 6/3	Massive	Very hard	None	Common

Results and Discussion

Distribution of Redoximorphic Pedofeatures

Table 2.3 presents the size distribution of sieved Fe–Mn nodules. The greatest content of the nodules is generally in the upper part of the profile (A, AEg, and Eg horizons). However, the Storozhynets profile is partially formed from the flysch residue and, in this profile, the greatest content of nodules (16.41 g kg^{-1}) is present in the 2Btg horizon, coinciding with the highest bulk density—which is responsible for periodic stagnation of water and frequent redox processes. A second maximum of nodules in the AEg horizon (12.98 g kg^{-1}) indicates the influence of the fragipan on the infiltration of water (Table 2.2).

In the other profiles, the concentration of Fe–Mn nodules in the upper solum suggests that the most frequent redox cycles occur above illuvial horizons. On the one hand, this is connected with the low permeability of the fragipan which causes a perched water table; on the other hand, the upper layers show the highest content of organic matter and are the most active biologically. The distribution of nodules also suggests that eluvial horizons have a higher content of hard nodules resistant to dissolution, which agrees with the data for Alfisols and Albeluvisols presented by Lindbo et al. (2000), Zhang and Karathanasis (1997), and Szymański and Skiba (2013). Table 2.4 presents the distribution of all Fe–Mn nodules (not only the coarser nodules separated by sieving) obtained from image analysis of micrographs.

Most nodules occur in illuvial horizons (Btx or Btg), coinciding with the higher content of iron (oxyhydr)oxides in lower soil horizons (Table 2.2). Iron (oxyhydr) oxides from upper soil horizons are eluviated to lower horizons, or accumulate as coarse nodules, or form organo-mineral complexes. In illuvial horizons, iron (oxyhydr)oxides form fine, soft nodules that dissolve easily, or they occur as irregular iron hypocoatings. This suggests that illuvial horizons are saturated with water for longer periods than eluvial horizons. This is related to their greater clay content (Table 2.2) and, also, drying of the upper layers by tree roots. Thus, an

Table 2.2 Physical and chemical properties of the studied soils

Horizon	Depth (cm)	Sand (%) (1–0.05 mm)	Silt (%) (0.05–0.002 mm)	Clay (%) (<0.002 mm)	Db[a] (Mg/m^3)	P[b] (%)	SOC[c] (%)	pH (H_2O)	Fe_o[d] (%)	Al_o[e] (%)
Storozhynets										
O	0–5	n.a.[f]	n.a.	n.a.	n.a.	n.a.	n.a.	n.a.	n.a.	n.a.
AEg	5–22	17.0	66.0	17.0	1.29	48.4	2.4	4.5	1.49	0.04
Eg	22–33	14.0	63.0	23.0	1.39	44.2	0.6	4.9	1.59	0.04
Btx	33–60	12.0	52.0	36.0	1.53	39.5	0.6	5.3	1.96	0.07
2Btg	60–100	19.0	34.0	47.0	1.58	37.3	0.5	5.6	2.21	0.07
2BC	100–140	13.0	33.0	54.0	1.55	37.6	n.a.	n.a.	n.a.	n.a.
Ispas										
O	0–3	n.a.	n.a.	n.a.	n.a.	n.a.	n.a.	n.a.	n.a.	n.a.
AEg	3–21	26.0	54.0	20.0	1.01	58.4	2.6	4.7	1.39	0.05
Eg	21–35	21.0	56.0	23.0	1.37	44.8	0.9	4.7	1.41	0.05
Btx1	35–52	19.0	49.0	32.0	1.41	42.2	0.6	4.7	1.66	0.06
Btx2	52–110	22.0	49.0	29.0	1.46	40.3	0.6	4.7	1.88	0.07
Btg	110–140	22.0	50.0	28.0	1.46	39.9	0.5	5.1	1.92	0.06
Mysliv										
O	0–2	n.a.	n.a.	n.a.	n.a.	n.a.	n.a.	n.a.	n.a.	n.a.
A	2–14	14.0	71.0	15.0	1.30	49.4	2.5	4.8	1.22	0.04
Eg	14–30	11.0	68.0	21.0	1.30	46.1	1.3	5.4	1.49	0.05
Btx1	30–49	10.0	64.0	26.0	1.37	42.3	1.0	5.3	1.74	0.05
Btx2	49–57	11.0	64.0	25.0	1.46	40.2	0.6	5.4	1.73	0.06

(continued)

Table 2.2 (continued)

Horizon	Depth (cm)	Sand (%) (1–0.05 mm)	Silt (%) (0.05–0.002 mm)	Clay (%) (<0.002 mm)	Db[a] (Mg/m^3)	P[b] (%)	SOC[c] (%)	pH (H_2O)	Fe_o[d] (%)	Al_o[e] (%)
Btg	57–120	10.0	73.0	17.0	1.67	35.6	0.4	5.0	1.98	0.06
Piilo										
O	0–6	n.a.	n.a.	n.a.	n.a.	n.a.	n.a.	n.a.	n.a.	n.a.
A	6–16	17.0	63.0	20.0	n.a.	n.a.	3.7	4.8	0.81	0.03
AE	16–31	n.a.	n.a.	n.a.	n.a.	n.a.	n.a.	n.a.	n.a.	n.a.
Eg	31–43	16.0	66.0	18.0	n.a.	n.a.	0.8	4.9	1.55	0.05
Btx1	43–72	16.0	62.0	22.0	n.a.	n.a.	0.5	5.1	1.64	0.07
Btx2	72–110	17.0	58.0	25.0	n.a.	n.a.	n.a.	5.2	1.57	0.05
BC	110–123	n.a.	n.a.	n.a.	n.a.	n.a.	n.a.	n.a.	n.a.	n.a.

[a]*Db* Bulk density
[b]*P* Total porosity
[c]*SOC* Soil organic carbon
[d]Fe_o Ammonium oxalate extractable Fe
[e]Al_o Ammonium oxalate extractable Al
[n.a.] Not analysed

Table 2.3 Distribution of hard Fe–Mn nodules

Horizon	Depth (cm)	1.0–0.5 mm	0.5–0.25 mm	0.25–0.10 mm	Sum
		g kg^{-1}			
Storozhynets					
O	0–5	n.a.[a]	n.a.	n.a.	n.a.
AEg	5–22	6.30	3.35	3.33	12.98
Eg	22–33	3.14	2.40	2.63	8.17
Btx	33–60	2.07	1.95	1.85	5.87
2Btg	60–100	7.16	3.95	5.30	16.41
2BC	100–140	1.01	0.75	1.75	3.51
Ispas					
O	0–3	n.a.	n.a.	n.a.	n.a.
AEg	3–21	24.42	8.05	5.20	37.67
Eg	21–35	9.46	6.65	4.03	20.14
Btx1	35–52	4.06	1.73	2.08	7.86
Btx2	52–110	2.18	2.40	2.17	6.75
Btg	110–140	1.66	1.43	2.65	5.73
Mysliv					
O	0–2	n.a.	n.a.	n.a.	n.a.
A	2–14	2.93	4.70	10.00	17.63
Eg	14–30	2.85	1.73	2.05	6.63
Btx1	30–49	2.74	1.98	2.58	7.29
Btx2	49–57	1.03	1.73	1.28	4.03
Btg	57–120	5.65	4.85	3.63	14.13
Piilo					
O	0–6	n.a.	n.a.	n.a.	n.a.
A	6–16	4.59	2.98	2.58	10.14
AE	16–31	n.a.	n.a.	n.a.	n.a.
Eg	31–43	11.38	3.50	2.53	17.41
Btx1	43–72	6.79	2.50	1.95	11.24
Btx2	72–110	3.55	2.40	3.18	9.12
BC	110–123	1.60	0.95	2.00	4.55

[a]*n.a.* Not analysed

analysis of the content, size, and shape of Fe–Mn nodules in soils provides information on the duration of waterlogging.

Micromorphology

Using Stoops' terminology (2003), Albeluvisols are characterized by intrusive redox pedofeatures (Fe and Fe–Mn coatings on the walls of voids and ped faces),

Table 2.4 Content of Fe–Mn pedofeatures according to percentage area in thin section

Horizon	Depth (cm)	Fe–Mn nodules and hypo- and quasicoatings (%)	Fe–Mn nodules (%)	Hypo- and quasicoatings (%)
Storozhynets				
O	0–5	n.a.[a]	n.a.	n.a.
AEg	5–22	19.27	7.87	11.40
Eg	22–33	9.50	6.50	3.01
Btx	33–60	36.19	17.35	18.84
2Btg	60–100	37.25	19.79	17.47
2BC	100–140	n.a.	n.a.	n.a.
Ispas				
O	0–3	n.a.	n.a.	n.a.
AEg	3–21	13.47	8.47	5.00
Eg	21–35	20.33	11.59	8.74
Btx1	35–52	18.83	8.10	10.73
Btx2	52–110	26.55	16.54	10.01
Btg	110–140	22.18	15.71	6.47
Mysliv				
O	0–2	n.a.	n.a.	n.a.
A	2–14	9.86	2.93	6.93
Eg	14–30	10.98	6.70	4.28
Btx1	30–49	33.91	23.15	10.75
Btx2	49–57	4.80	4.17	0.63
Btg	57–120	n.a.	n.a.	n.a.
Piilo				
O	0–6	n.a.	n.a.	n.a.
A	6–16	18.08	7.21	11.46
Eg	31–43	15.49	5.65	9.84
Btx1	43–72	18.03	13.72	4.31
Btx2	72–110	14.19	8.24	5.95
BC	110–123	12.06	6.86	5.30

[a]*n.a.* Not analysed

impregnative pedofeatures (Fe–Mn nodules and iron and iron–manganese hypo- and quasicoatings), and depletion pedofeatures (zones lighter in colour due to removal of Fe (oxyhydr)oxides and Mn oxides). Iron and iron–manganese coatings occur only in illuvial horizons (fragipan and argillic, Fig. 2.2a, b). Some may also be related to migration of iron and manganese within illuvial horizons when the soil is saturated long enough to reduce the iron (oxyhydr)oxides and manganese oxides (Vepraskas et al. 2006). The Fe–Mn coatings do not show Fe-enriched and

Mn-enriched layers which might indicate a rapid shift from reduced to oxidized conditions (Huang et al. 2008). And Fe-rich clay coatings in illuvial horizons suggest simultaneous migration of iron (oxyhydr)oxides and clay particles (Nikorych et al. 2014).

Two main types of Fe–Mn nodules are observed: (1) orthic nodules showing undifferentiated internal fabric and gradual boundaries (Fig. 2.3a, b) and (2) orthic nodules showing undifferentiated internal fabric and sharp boundaries (Fig. 2.3c–f).

The orthic nodules consist of iron (oxyhydr)oxides and manganese oxide, quartz grains, humus (especially in upper soil horizons), and clay minerals (especially in illuvial horizons). They are similar to Fe–Mn nodules found in Albeluvisols in the Carpathian foothills of southern Poland described by Szymański and Skiba (2013). Orthic, irregular nodules are the most common in all of the studied soil profiles (Fig. 2.3a, b); they are most abundant in illuvial horizons (Btx and Btg) but are also present in upper horizons (A, AEg, Eg). Undifferentiated internal fabric (the same as the matrix) and gradual boundaries indicate that the nodules formed in situ—presumably by periodic water saturation leading to the reduction of Fe and Mn compounds and subsequent desaturation, oxidation, and precipitation as Fe (oxyhydr)oxides and Mn oxides. This implies that the nodules are not relict features but are forming now (Hseu and Chen 1996; Vepraskas 2004, Szymański and Skiba 2013). Disorthic nodules also occur in the upper part of the studied soils (A, AEg,

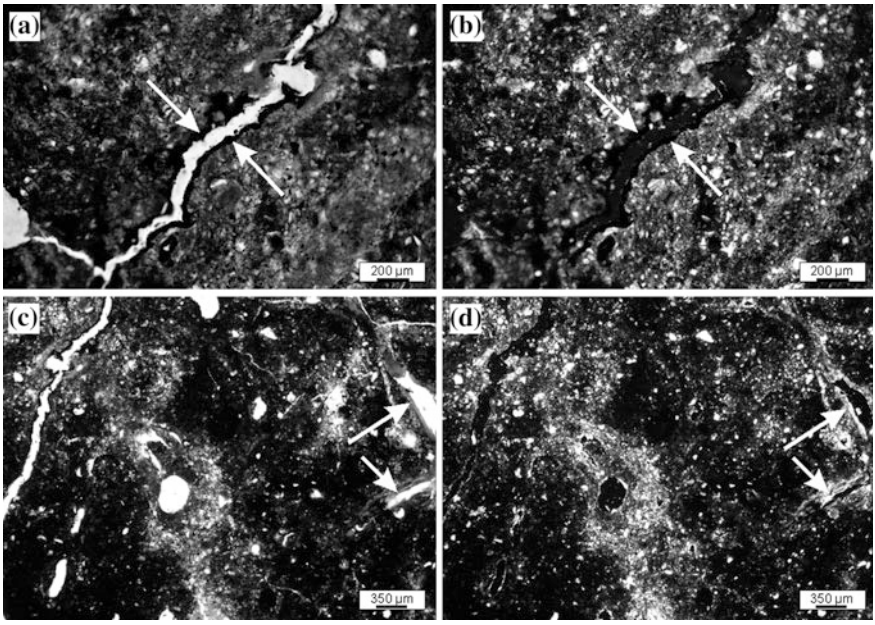

Fig. 2.2 Storozhynets profile: Fe–Mn coatings (*white arrows*) in fragipan (Btx) (**a**, **b**). Iron depletion and iron impregnative hypocoatings and clay coatings (*white arrows*) in fragipan (Btx) (**c**, **d**). Plane polarized light (**a**, **c**) and crossed polarized light (**b**, **d**)

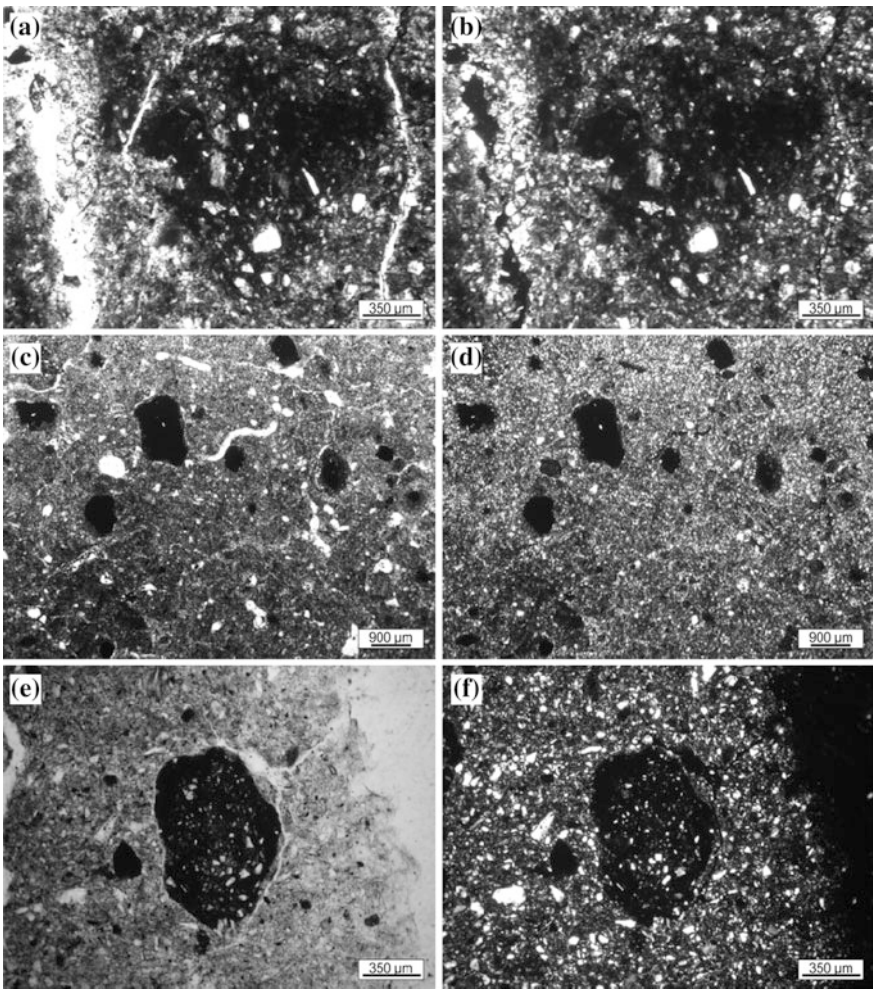

Fig. 2.3 Micromorphology of orthic Fe–Mn nodules: with gradual boundary in fragipan from the Ispas profile (**a**, **b**); with sharp boundary in eluvial horizon from the Piilo profile (**c**, **d**); and with a sharp boundary in eluvial horizon from the Storozhynets profile (**e**, **f**). Plane polarized light (**a**, **c**, **e**) and crossed polarized light (**b**, **d**, **f**)

and Eg horizons); they might form from orthic nodules that have been displaced by faunal mixing of soil material.

In addition to Fe–Mn nodules, impregnative and depletion hypocoatings occur in the illuvial horizons (Fig. 2.2c, d). These features are also related to cyclic reduction and oxidation (Vepraskas 2004; Lindbo et al. 2010; Nikorych et al. 2014). Iron and iron–manganese depletion hypocoatings occur mainly along vertical cracks and channels, indicating that they relate to flowing water containing dissolved organic matter (DOM) that is a source of energy for the microorganisms

responsible for reduction. In many cases, clay depletion hypocoatings are associated with Fe and Fe–Mn depletion hypocoatings; the reduction and eluviation of iron (oxyhydr)oxides and manganese oxides facilitates dispersion and translocation of clay. In turn, eluvial horizons are characterized by bleaching that indicates depletion of iron (oxyhydr)oxides and manganese oxides. The process is linked with illuvial horizons of low hydraulic conductivity and periodic stagnation of water table above them. Reduction and depletion of iron (oxyhydr)oxides and manganese oxides is also related to the concentration of organic matter in the upper soil and the greater porosity of the upper solum, compared with the illuvial horizons, which facilitates the migration of water containing DOM (Vepraskas 2004).

Chemical Composition of Fe–Mn Nodules

The main constituents of Fe–Mn nodules are SiO_2 (55.0–62.5%), Fe_2O_3 (20.1–27.8%), Al_2O_3 (7.1–10.1%), MnO (1.1–4.0%), K_2O (1.2–1.9%), and P_2O_5 (0.6–1.9%); other constituents rarely exceed 1% (Table 2.5). The data are similar to those obtained by Zhang and Karathanasis (1997), Tan et al. (2006), and Szymański and Skiba (2013) for soils in Kentucky (USA), various parts of China, and the Carpathian foothills in Poland, respectively. The content of SiO_2 in Fe–Mn nodules shows a uniform distribution throughout the profile with only small variance (2–4%) between horizons; the content of Al_2O_3 follows a similar pattern with variance from 1 to 3%, but the Al_2O_3 content of Fe–Mn nodules is slightly higher in the fragipan, most likely linked with a higher content of clay minerals in illuvial horizons (Nikorych et al. 2014).

At first sight, the distribution of Fe_2O_3 and MnO in the nodules shows no particular pattern, suggesting that there is no relationship between the quantity of the nodules and content of Fe and Mn in the soil profile. However, on summation of the Fe and Mn content, their joint distribution becomes uniform—variances do not exceed 2%, with the exception of the Piilo profile (coefficient of variation 5%). The chemical data for the nodules show that if the nodules from the eluvial horizon contain a larger amount of Fe in comparison with nodules obtained from the illuvial horizon, then the content of Mn in nodules obtained from the eluvial horizon is lower than in nodules obtained from the illuvial horizon, and vice versa (except the Mysliv profile). However, this is only a tendency and not a regular pattern, as indicated by relatively high coefficients of variation (10–50% for Fe_2O_3 and almost 100% for MnO).

Enrichment factors (EF) vary according to the element. The content of Si and Al in the nodules is lower than in the surrounding soil material (EF < 1) likewise for Mg, K, and Na. On the other hand, the nodules are enriched in Fe (4–14 times) and especially in Mn (7–40 times) in comparison with the surrounding soil material (Table 2.6). This agrees with data presented by Tan et al. (2006), for Chinese soils, and Palumbo et al. (2001), for Sicilian soils.

Table 2.5 Chemical composition of Fe–Mn nodules obtained using SEM–EDS

Horizon	Depth (cm)	SiO_2 (%)	Al_2O_3 (%)	Fe_2O_3 (%)	MnO (%)	CaO (%)	MgO (%)	K_2O (%)	Na_2O (%)	P_2O_5 (%)	SO_3 (%)	TiO_2 (%)	Cr_2O_3 (%)	CoO (%)	NiO (%)	CuO (%)	ZnO (%)
Storozhynets																	
Eg	22–33	55.82	7.44	27.68	1.30	1.27	0.36	1.43	0.73	1.31	1.47	0.52	0.12	0.12	0.17	0.07	0.18
Btx	33–60	57.08	9.87	23.75	3.31	1.02	0.60	1.71	0.62	0.57	0.41	0.46	0.04	0.16	0.16	0.04	0.19
2Btg	60–100	58.34	7.85	27.08	1.82	0.72	0.31	1.24	0.50	0.81	0.36	0.54	0.05	0.08	0.11	0.07	0.13
Ispas																	
Eg	21–35	58.55	8.55	26.00	1.56	0.49	0.42	1.70	0.61	0.66	0.38	0.67	0.08	0.15	0.06	0.05	0.08
Btx1	35–52	56.85	10.40	23.28	4.01	0.53	0.58	1.74	0.65	0.78	0.37	0.49	0.07	0.08	0.07	0.07	0.04
Mysliv																	
Eg	14–30	57.39	8.70	26.10	1.12	1.21	0.51	1.75	0.75	1.07	0.43	0.46	0.10	0.09	0.07	0.07	0.15
Btx1	30–49	53.99	9.58	27.65	1.84	1.26	0.61	1.91	0.79	0.98	0.40	0.55	0.05	0.16	0.08	0.06	0.10
Btg	57–120	58.67	7.13	26.19	1.10	0.77	0.37	1.76	1.01	1.59	0.33	0.46	0.02	0.12	0.13	0.16	0.19
Piilo																	
Eg	31–43	62.52	7.20	20.12	3.21	0.63	0.29	1.75	0.65	1.91	0.43	0.69	0.27	0.13	0.04	0.02	0.14
Btx1	43–72	56.13	8.05	27.78	1.16	0.78	0.40	1.79	0.56	1.74	0.81	0.41	0.11	0.01	0.06	0.13	0.08

Table 2.6 EF for selected elements in Fe–Mn nodules in relation to the elements in surrounding soil material

Horizon	Depth (cm)	SiO_2	Al_2O_3	Fe_2O_3	MnO	CaO	MgO	K_2O	Na_2O
Storozhynets									
Eg	22–33	0.70	0.93	10.48	7.22	3.63	0.33	0.79	0.63
Btx	33–60	0.83	0.78	4.91	33.1	2.22	0.44	0.95	0.89
2Btg	60–100	0.92	0.54	4.26	10.11	1.38	0.25	0.59	0.45
Ispas									
Eg	21–35	0.80	0.66	14.29	9.75	0.68	0.49	0.89	0.60
Btx1	35–52	0.79	0.74	5.91	33.42	0.63	0.57	0.95	0.83
Mysliv									
Eg	14–30	0.72	1.10	10.70	22.40	5.04	0.78	0.85	0.76
Btx1	30–49	0.72	0.97	6.39	15.33	3.60	0.62	0.89	0.88
Btg	57–120	0.81	0.69	6.40	7.33	1.31	0.38	0.77	1.23
Piilo									
Eg	31–43	0.79	0.97	6.27	40.13	2.63	0.45	0.88	0.79
Btx1	43–72	0.73	0.93	7.91	14.50	1.70	0.32	0.85	0.66

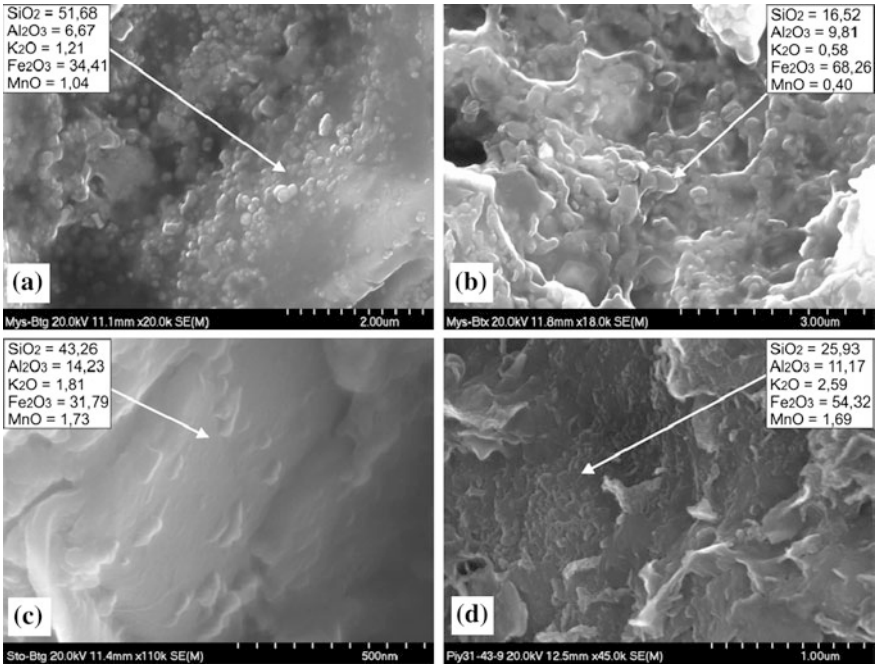

Fig. 2.4 Surface of Fe–Mn nodules from Btx1 and Btg horizons in the Mysliv profile (**a**, **b**), from Btg horizon in the Storozhynets profile (**c**), and from Eg horizon in the Piilo profile (**d**) with microbial cells and content of selected elements (SEM–EDS)

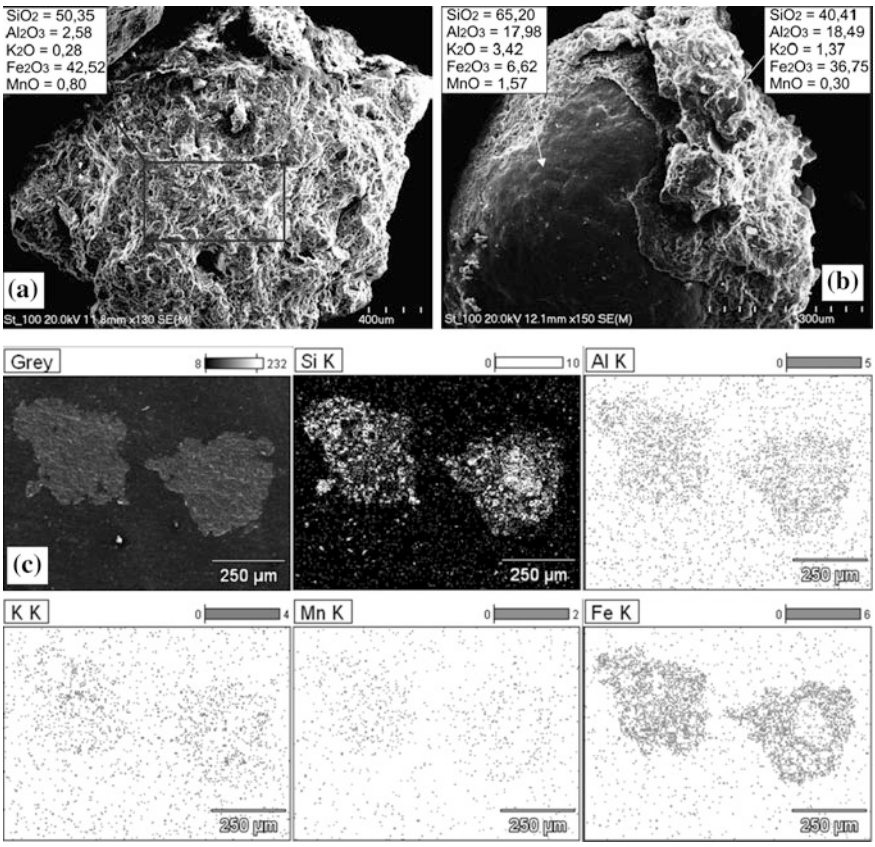

Fig. 2.5 Typic, orthic Fe–Mn nodule (**a**) and concretion showing concentric crusts (**b**), and content of selected elements in both pedofeatures from 2BC horizon of the Storozhynets profile; section of typic, orthic Fe–Mn nodule (**c** *left*) and nucleic Fe–Mn nodule (**c** *right*), and spatial distribution of selected elements in the both nodules from Eg horizon of the Piilo profile (SEM–EDS)

The mechanism of formation of Fe–Mn nodules might be biological and/or chemical (Timofeeva and Golov 2010). The weak correlation between the quantity of nodules and their content of Fe and Mn (for Fe_2O_3, r = –0.22; for MnO, r = –0.09) suggests a biological origin. Chemotrophic bacteria form local colonies or films, depending on micro-conditions, and the different quality and quantity of soil microorganism communities lead to variability in the content of Fe and Mn in nodules. The physiological manner of deposition of these elements in microbial cells—depending on specific local conditions—may also play a role (Timofeeva and Golov 2010). Specific local conditions may occur within the same soil horizon; for example, during strong anaerobiosis in any particular horizon, there are always micro-sites containing oxygen, and vice versa (Aristovskaya 1980).

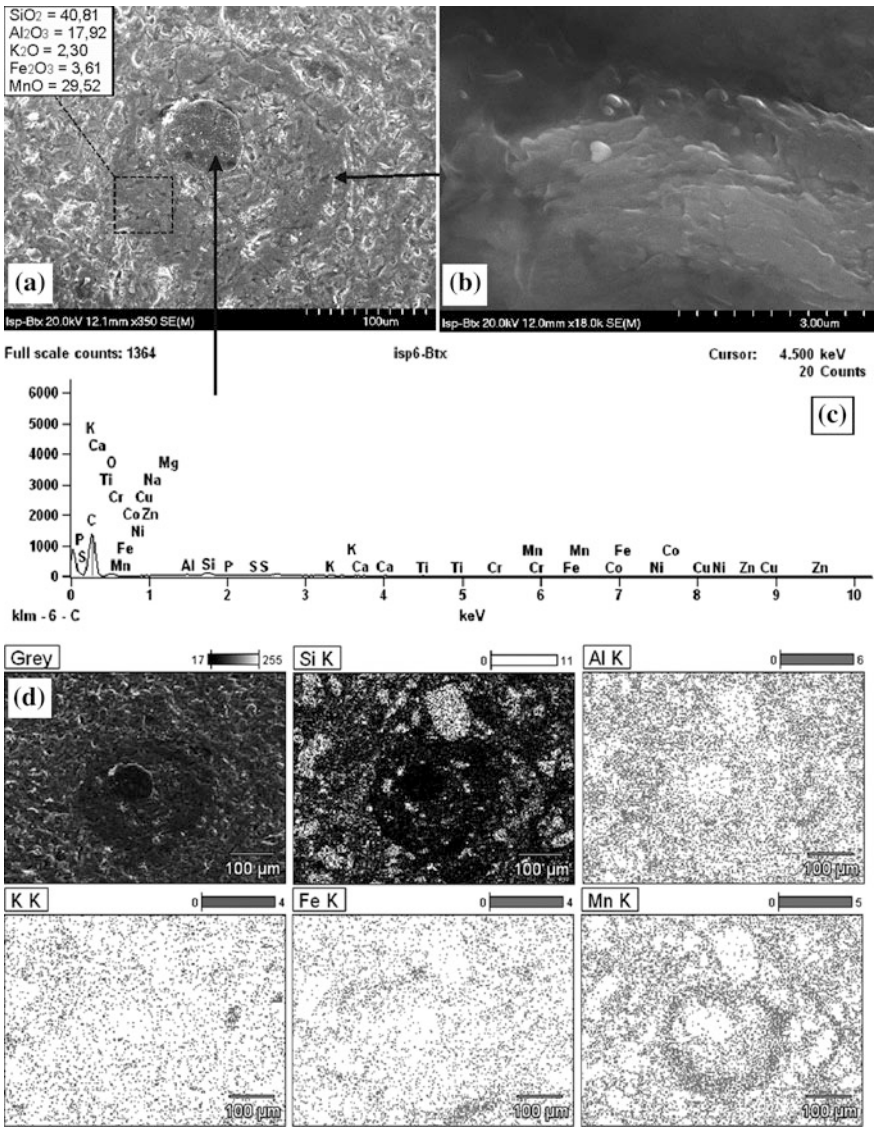

Fig. 2.6 Internal structure of Fe–Mn concretion showing concentric band enriched in Mn (**a**), presence of microorganisms in the band (**b**), chemical composition of centre (probably fungal hyphae) of the pedofeature (**c**), and spatial distribution of selected elements in the pedofeature (**d**) from Btx1 horizon of the Ispas profile (SEM–EDS)

Figure 2.4 shows the porous, pitted surface of an Fe–Mn nodule covered with microbial cells. The surface of the nodule in contact with these microorganisms has a high content of Fe and Mn; in other places, the content of Fe and Mn is lower

(~50%), which suggests that micro-organisms play a crucial role in the accumulation of Fe and Mn, leading to the formation of nodules.

Two main types of Fe–Mn nodules are observed. The internal fabric of almost all of the studied nodules indicates that the nodules are micro-aggregates (Fig. 2.5a) with a high content of relatively uniformly distributed Fe and Mn (Fig. 2.5c left nodule).

However, some of the nodules (concretions) are characterized by concentric layers that have larger quantities of Fe and Mn (Fig. 2.5b, c right nodule). Such a concentric internal structure indicates cyclic formation of the nodule, which we may attribute to periodic wet and dry periods. During the wet season (and reducing conditions because of lack of oxygen), both Fe and Mn shift to a soluble, reduced state and migrate with the soil solution. When the soil begins to dry (and oxidation predominates), both Fe and Mn are oxidized and deposited onto a variety of morphological features such as the walls of pores, faces of aggregates, and mineral grains (Huang et al. 2008). Repetition of these cycles leads to the formation of a concentric internal structure of Fe–Mn nodules and their seasonal growth (Fig. 2.6) (Manceau et al. 2003).

Conclusions

The studied Albeluvisols are characterized by intrusive redox pedofeatures, impregnative redox pedofeatures, and depletion redox pedofeatures. Orthic nodules of undifferentiated internal fabric and gradual boundaries are most common; orthic nodules showing undifferentiated internal fabric and sharp boundaries also occur. Additionally, illuvial horizons exhibit Fe–Mn coatings as well as impregnative and depletion hypocoatings—the latter mainly along vertical cracks and channels.

The concentration of coarse, hard Fe–Mn nodules in the upper part of the soil profiles indicates that cyclic redox processes occur most often above illuvial horizons. This is linked with the low permeability of the fragipan, leading to periodic formation of a perched water table, as well as the greater content of organic matter in the upper layers. However, the highest content of all nodules (not only coarse nodules) occurs in illuvial horizons (Btx or Btg). This is related to a higher content of iron (oxyhydr)oxides in lower soil horizons and their longer periods of waterlogging compared with eluvial horizons.

Fe–Mn nodules are composed mainly of SiO_2, Fe_2O_3, Al_2O_3, MnO, K_2O, and P_2O_5. The content of Si, Al, Mg, K, and Na in the nodules is lower than that in the surrounding soil material. On the other hand, the nodules are enriched in Fe (4–14 times) and especially in Mn (7–40 times) compared with the surrounding soil material. The chemical composition and spatial distribution of the main components of Fe–Mn pedofeatures indicate the occurrence of two types of pedofeatures: nodules and concretions, nodules being much more common.

The crucial role of microorganisms in the accumulation of Fe and Mn in nodules is demonstrated by the distinctive chemical composition of the nodule surface in contact with microorganisms.

References

Aristovskaya TV (1980) Microbiology of soil formation processes. Nauka, Leningrad (Russian)
Brewer R (1964) Fabric and mineral analysis of soils. Wiley, New York
Cornu S, Cattle JA, Samouëlian A et al (2009) Impact of redox cycles on manganese, iron, cobalt, and lead in nodules. Soil Sci Soc Am J 73:1231–1241
Dawson BSW, Ferguson JE, Campbell AS, Cutler EJB (1985) Distribution of elements in some Fe–Mn nodules and an iron-pan in some gley soils of New Zealand. Geoderma 35:127–143
Gasparatos D, Tarenidis D, Haidouti D, Oikonomou G (2005) Microscopic structure of soil Fe–Mn nodules: environmental implications. Environ Chem Lett 2:175–178
Hickey PJ, McDaniel PA, Strawn DG (2008) Characterization of iron–manganese cemented redoximorphic aggregates on wetland soils contaminated with mine wastes. J Environ Qual 37:2375–2385
Hseu ZY, Chen ZS (1996) Saturation, reduction and redox morphology of seasonally-flooded Alfisols in Taiwan. Soil Sci Soc Am J 60:941–949
Huang L, Hong J, Tan W et al (2008) Characteristics of micromorphology and element distribution of iron-manganese cutans in typical soils of subtropical China. Geoderma 146:40–47
IUSS Working Group WRB (2006) World reference base for soil resources 2006. World Soil Resources Reports 103, FAO, Rome
IUSS Working Group WRB (2014) World reference base for soil resources 2014. World Soil Resources Reports 106, FAO, Rome
Latrille C, Elsass F, van Oort F, Denaix L (2001) Physical speciation of trace metals in Fe-Mn concretions from a rendzic lithosol developed on Sinemurian limestones (France). Geoderma 100:127–146
Lindbo DL, Rhoton FE, Hudnall WH et al (2000) Fragipan degradation and nodule formation in Glossic Fragiudalfs of the Lower Mississippi River Valley. Soil Sci Soc Am J 64:1713–1722
Lindbo DL, Stolt MH, Vepraskas MJ (2010) Redoximorphic features. In: Stoops G, Marcelin V, Mees F (eds) Interpretation of micromorphological features of soils and regoliths. Elsevier, Amsterdam, pp 129–147
Manceau A, Tamura N, Celestre RS et al (2003) Molecular-scale speciation of Zn and Ni in soil ferromanganese nodules from loess soils of the Mississippi basin. Environ Sci Technol 37:75–80
Nelson DW, Sommers LE (1996) Total carbon, organic carbon, and organic matter. In: Sparks DL et al. (eds) Methods of soil analysis. Part 3. Chemical methods. SSSA Book Series, vol 5. SSSA and ASA, Madison, pp 961–1010
Nikorych V, Szymański W, Polchyna S, Skiba M (2014) Genesis and evolution of the fragipan in Albeluvisols in the Precarpathians in Ukraine. Catena 119:154–165
Palumbo B, Bellanca A, Neri R, Roe MJ (2001) Trace metal partitioning in Fe–Mn nodules from Sicilian soils, Italy. Chem Geol 173:257–269
Quénard L, Samouëlian A, Laroche B, Cornu S (2011) Lessivage as a major process of soil formation: a revisition of existing data. Geoderma 167–168:135–147
Schwertmann U, Fanning DS (1976) Iron-manganese concretions in hydrosequences of soils in loess in Bavaria. Soil Sci Soc Am J 40:731–773
Sipos P, Németh T, May Z, Szalai Z (2011) Accumulation of trace elements in Fe-rich nodules in a neutral-slightly alkaline floodplain soil. Carpathian J Earth Environ Sci 6(1):13–22

Stoops G (2003) Guidelines for analysis and description of soil and regolith thin sections. SSSA, Madison

Suarez DL, Langmuir D (1976) Heavy metals in a Pennsylvania soil. Geochim Cosmochim Acta 40:589–598

Szendrei G, Kovács-Pálffy P, Földvari M, Gál-Sólymos K (2012) Mineralogical study of ferruginous and manganiferous nodules separated from characteristic profiles of hydromorphic soils in Hungary. Carpathian J Earth Environ Sci 7(1):59–70

Szymański W, Skiba M (2013) Distribution, morphology and chemical composition of Fe–Mn nodules in Albeluvisols of the Carpathian Foothills, Poland. Pedosphere 23(4):445–454

Tan WF, Liu F, Li YH et al (2006) Elemental composition and geochemical characteristics of iron-manganese nodules in main soils of China. Pedosphere 16:72–81

Timofeeva YO, Golov VI (2010) Accumulation of microelements in iron nodules in concretions in soils: a review. Eurasian Soil Sci 43(4):434–440

Vepraskas MJ (2001) Morphological features of seasonally reduced soils. In: Richardson JL, Vepraskas MJ (eds) Wetland soils: genesis, hydrology, landscapes and classification. Lewis Publishers, Boca Raton, pp 163–182

Vepraskas MJ (2004) Redoximorphic features for identifying aquic conditions. Technical Bulletin 301, North Carolina Agricultural Research Service, Raleigh

Vepraskas MJ, Richardson JL, Tandarich JP (2006) Dynamics of redoximorphic feature formation under controlled ponding in a created riverine wetland. Wetlands 26:486–496

Zaidelman FR, Nikiforova AS (2001) Genesis and diagnostic meaning of soil neoformations of forest and forest-steppe zones. Moscow University Press (Russian)

Zaidelman FR, Nikiforova AS (2010) Ferromanganese concretionary neoformations: a review. Eura Soil Sci 43:248–258

Zhang M, Karathanasis AD (1997) Characterization of iron-manganese concretions in Kentucky Alfisols with perched water tables. Clays Clay Miner 45:428–439

http://www.springer.com/978-3-319-45416-0

Soil Science Working for a Living
Applications of soil science to present-day problems
Dent, D.; Dmytruk, Y. (Eds.)
2017, XIII, 290 p. 89 illus., 50 illus. in color., Hardcover
ISBN: 978-3-319-45416-0